5-2020

# Optical Metabolic Imaging as a Predictor of Patient Tumor Response to Therapy and Apoptosis

Andrew Larey

# Optical Metabolic Imaging as a Predictor of Patient Tumor Response to Therapy and Apoptosis

**Honors Thesis**

**Andrew Larey, Honors Biomedical Engineering[1]; Timothy Muldoon, Ph.D.[1]**

**[1]Department of Biomedical Engineering, University of Arkansas, Fayetteville, AR**

**Spring 2020**

**Abstract**

Despite a plethora of medical advancements, malignant tumors remain difficult to treat due to complex cancer biology and interpatient heterogeneity. Phenotypically similar tumors may respond differently to a given treatment. In clinical oncology, it is paramount to quantify tumor response to therapy for predicting treatment outcome, monitoring tumor changes, identifying effective therapies, and avoiding unnecessary cost and toxicity to the patient. Current standards of monitoring tumor response to therapy include CT, MRI, PET, and histopathology; these methods either take a merely anatomical approach or are invasive and time consuming, necessitating a functional biomarker approach. MPM represents a metabolic-level method of effectively quantifying tumor response that is noninvasive and achieves high spatial resolution and increased imaging depth. This thesis pursued creation of a benchmark for 5-FU-induced apoptosis in CRC cells based on CC3 frequency in order to use this marker to verify TPEFM as an *ex vivo* method of quantifying patient-specific CRC tumor response to 5-FU via changes in optical redox ratio as an indicator of apoptosis. Lack of sensitivity of the Western blot protocol to CC3 precluded accurate quantification of CC3 frequency over 5-FU exposure times and concentrations. Significant changes in redox ratio throughout 5-FU exposure times were observed but may remain inconclusive when considering the metabolic properties of most cancers. Although redox ratio imaging was successfully conducted here, redox ratio data was not correlated with a reliable marker of apoptosis in the same context. With further apoptosis assays and more rigorous exploration of the relationship of redox ratio, the metabolic profile of CRC cells, and 5-FU-induced apoptosis in CRC cells, TPEFM may be established as a high-resolution metabolic technique for monitoring treatment effectiveness in this context and with novel drugs and other cancer types.

## Introduction

### Problem Overview and Current Approaches

Approximately 38% of men and women will be diagnosed with cancer at some point in their life, and the U.S. national expenditure for care totaled $147 billion in 2017. (1) Furthermore, cancerous tumors with apparently similar phenotypes may not respond identically to a given treatment, a testament to current limits in the understanding of the complexity of tumor biology and how this biology determines tumor response to a given therapy. (1) It remains that measuring tumor response to therapy is vital in clinical oncology for predicting treatment outcome, monitoring tumor changes, identifying effective therapies, and avoiding unnecessary cost and toxicity. (2) Thus, it becomes necessary to monitor cancer treatment efficacy at an individual level due to complex tumor biology and interpatient heterogeneity.

Current standards for quantifying tumor response to therapy include measuring tumor shrinkage through imaging (CT, MRI, PET), a method that suffers from interobserver variability, difficult differentiation of non-viable tumor and fibrotic tissue from malignant tumor, and inadequate spatial resolution to quantify changes at the subcellular level. (3) Furthermore, tumor shrinkage may not always be indicative of treatment effectiveness. This issue also arises in drug testing: tumor response to therapy is a useful surrogate for clinical benefit of new drugs, but current tumor shrinkage criteria may not be beneficial for assessing the efficacy of drugs with novel mechanisms of action. (1) Additional histopathological methods involve invasive needle biopsies that suffer from sampling error and time-consumption. (2-4) Lastly, serum markers for treatment effectiveness tend to be present in low concentrations and thus may be misleading. (1) The ultimate indicator of treatment effectiveness is improvement in symptoms and survival; however, earlier and more objective/quantifiable metrics are necessary. Tumor response measurements should shift

from an anatomical approach to a functional-biomarker approach to achieve more objective information at the subcellular level and increase treatment efficiency by balancing treatment cost and efficacy through halting ineffective treatments and moving on to effective treatments faster. (3)

**Colorectal Cancer, 5-FU Chemotherapy, and Apoptosis**

Colorectal cancer (CRC) specifically is responsible for the third most cancer-related deaths in the U.S. and is the fourth most common cancer. (5, 6) Especially since it is generally considered incurable after metastasis, CRC is an example of a very common tumorigenic disease that could benefit from more effective methods of monitoring tumor response to therapy. (7) The current first line of treatment for CRC tumors is the chemotherapeutic drug 5-fluorouracil (5-FU), which serves to induce apoptosis in CRC cells. (8, 9) The 5-FU mechanism of action involves a metabolite of 5-FU complexing with thymidylate synthetase, preventing DNA synthesis. (9) The lack of DNA synthesis and repair is a key initiator of apoptosis through the intrinsic pathway, as the accumulation of DNA genotoxins results in the development of critical lesions, such as DNA double-stranded breaks, followed by caspase activation. (10, 11) Caspases are often used as markers of apoptosis due to their direct role in the apoptosis pathway. (2) Activation of effector caspases, such as caspase-3 (cleaved caspase-3 (CC3) in the activated form), is considered a reliable marker of apoptosis because the apoptosis pathway converges at effector caspases to proceed irreversibly to cell death via DNA, nuclear protein, and cytoskeletal protein degradation. This is followed by chromatin and cytoplasmic condensation, nuclear fragmentation, and, finally, formation of apoptotic bodies consisting of the cellular debris. (2) Thus, it remains that detection of CC3 in CRC cells that undergo 5-FU-induced apoptosis is a reliable and quantifiable marker of apoptosis activity and, consequently, treatment efficacy in the lab. (12)

## Multiphoton Microscopy and Optical Redox Ratio Imaging

Multi-photon microscopy (MPM) is a fluorescence microscopy method with two-photon excitation that permits superior 3-D image reconstruction with minimum photobleaching and background noise. (13) MPM allows imaging of live cellular processes with improved spatial resolution and precision at useful sampling depths. (13) Two-photon excitation fluorescence microscopy (TPEFM) is a metabolic-level method that can be used to quantify important sub-cellular autofluorescent metabolic cofactors, namely reduced nicotinamide adenine dinucleotide (NADH) and oxidized flavin adenine dinucleotide (FAD). (14) FAD and NADH occupy critical roles in facilitating oxidation-reduction reactions in glycolysis, the citric acid cycle, and oxidative phosphorylation. (14) Because FAD fluoresces in the oxidized form and NADH fluoresces in the reduced form with no exogenous fluorophores, these cofactors may be used to quantify tumor cell metabolism and changes thereto due to apoptosis by quantification of an optical oxidation-reduction ratio (redox ratio), indicative of metabolic activity. (14-16) Optical redox ratio essentially reports the ratio of oxidative phosphorylation to glycolysis as a metric of metabolic activity and consequent tumor characteristics. (4, 7, 12, 17-20) Thus, MPM is a method of effectively quantifying tumor response to disease treatment and novel drugs that is noninvasive, live, metabolic-level, and achieves high spatial resolution and increased imaging depth for monitoring of functional cellular changes. (4, 6, 7, 12, 21)

## Objectives

This thesis describes how MPM may be evaluated as a potential clinical means for quantifying tumor response by comparison with known markers of treatment success in the same context of cell line and chemotherapy. The objective is to create a standard for 5-FU-induced apoptosis in colorectal cancer cells by measuring the occurrence of CC3 in treated cells over time,

then evaluate MPM against the caspase standard as a potential *ex vivo* method to quantify patient-specific tumor response to 5-FU, specifically quantifying redox ratio as a marker for apoptosis frequency and thus treatment efficacy.

## Materials and Methods

### Cell Culture

HCT116 CRC cells (American Type Culture Collecation, VA, USA) taken from cryopreservation were expanded in a T-75 flask using standard cell culture procedures. Cells were incubated at 5% $CO_2$ and 37° C. Cells were fed every 48 hours with complete media consisting of McCoy's base media (Thermo Fisher Scientific Inc., Waltham, MA), 10% fetal bovine serum (American Type Culture Collecation, VA, USA), 1% penicillin-streptomycin (Sigma-Aldrich, St. Louis, MO), and 0.2% gentamicin/amphotericin (Thermo Fisher Scientific Inc., Waltham, MA).

### CC3 Western Blot

After expansion, cells were plated in 6-well plates at a density of $0.3x10^6$ cells/well. The cells were allowed to expand according to standard cell culture procedures to 80% confluence in the 6-well plates before being treated with 5-FU. Three control groups and 4 treatment groups were used in these experiments. The control groups consisted of 0 μM 5-FU treatment for exposure times of 0, 12, and 24 hours. The treatment groups consisted of 10 and 20 μM 5-FU treatment for exposure times of 12 and 24 hours. A 16-hour exposure time was also used in place of the 12-hour exposure time in some experiments to maintain consistency with timepoints used in other apoptosis assays being conducted in the lab. 5-FU doses were administered in solution with media, and the media was not changed during the treatment period. Treatment and control groups cells were harvested according to their respective exposure times: the cells were washed with dPBS,

unadhered with trypsin-EDTA, moved to a 15 mL conical tube, then centrifuged at 500 g for 5 minutes. Next, the supernatant was removed, and the cells rewashed with dPBS and centrifugation twice more before suspension in 1 mL of dPBS in an Eppendorf tube. The Eppendorf tube was centrifuged at 10,000 g for 5 minutes. The supernatant was removed, and the cells were resuspended in 100 µL of complete RIPA lysis buffer solution, then recentrifuged at 10,000 g for 5 minutes. The lysate collected was stored in a -80° C freezer until use in a BCA assay to quantify total protein content for preparation of Western blot samples.

Western blotting followed with an optimized CC3 blotting protocol with β-actin serving as a loading control (to control for lane variance) and a standard protein sample, or protein ladder, as an exposure control (to control for gel variance). 70 µg of protein was loaded for SDS-PAGE; the system ran at 200 V for approximately 45 minutes. Next, transfer took place at 4º C on ice for 20 hours at 10 V. Protein was transferred to a PVDF membrane with 0.2 µm pores. After transfer was complete, regions of interest were cut and blocked using a blocking buffer (Li-Cor) for 2 hours at room temperature. The regions of interest include CC3 fragments appearing at 17 and 19 kDa and β-actin, appearing at approximately 42 kDa. Primary antibody staining occurred at 4º C overnight. Secondary antibody staining was performed at room temperature for 1 hour. The membrane was then washed several times before imaging on an Odyssey near infrared scanner. Band quantification was attempted by densitometric analysis in ImageJ. Identical rectangular regions along the same axis were drawn around bands. Finally, band intensities were partitioned from background intensities on intensity histograms of the selected regions with little to no success.

**Multiphoton Microscopy of Optical Redox Ratio**

After expansion, cells were plated in 35 mm round, No. 1.5 coverslip MatTek glass-bottom dishes (MA, USA) at a density of $0.3x10^6$ cells/well. The cells were allowed to expand to 80%

confluence in the glass-bottom dishes before being treated with 5-FU. One control group and 2 treatment groups were used in these experiments. The control group consisted of 0 μM 5-FU treatment for an exposure time of 0 hours. The treatment groups consisted of 10 μM 5-FU treatment for exposure times of 16 and 24 hours. 5-FU doses were administered in solution with media, and the media was not changed during the treatment period. Cells were plated, expanded, and treated according to treatment group exposure times so that all groups could undergo MPM the same day. MPM redox ratio imaging was performed using a custom-built TPEFM. (4) Cell dishes were placed in a microincubator at standard conditions for the duration of imaging. Each field of view was comprised of two images: NADH intensity and FAD intensity. (4) The FAD channel was imaged with an excitation wavelength of 760 nm and an emission wavelength of 460 nm; the NADH channel was imaged with an excitation wavelength of 850 nm and an emission wavelength of 525 nm. Both channels were imaged with 60 mW of power at the sample, 100 gain, and 2X magnification for a 200-frame average at 58 frames/sec (256x256 pixel images, resolution=1.25 μm/pixel). Seven fields of view were imaged for the control group, 7 for the 16-hour treatment group, and 6 for the 24-hour treatment group. A custom CellProfiler pipeline (Version 3.1.9) was used to segment the cytoplasm of individual cells from nuclei and background and generate a mask based on NADH images. The NADH image mask was then applied to the FAD image in the same field of view. Redox ratio was then quantified on a per pixel basis using the channel intensity formula $\frac{FAD}{FAD+NADH}$ and the median redox ratio computed for individual cells.

## Results

### CC3 Western Blot

**Figure 1:** The CC3 Western blot reveals little to no fluorescence at 17 and 19 kDa relative to background noise and loading control, precluding accurate quantification of CC3 band intensity.

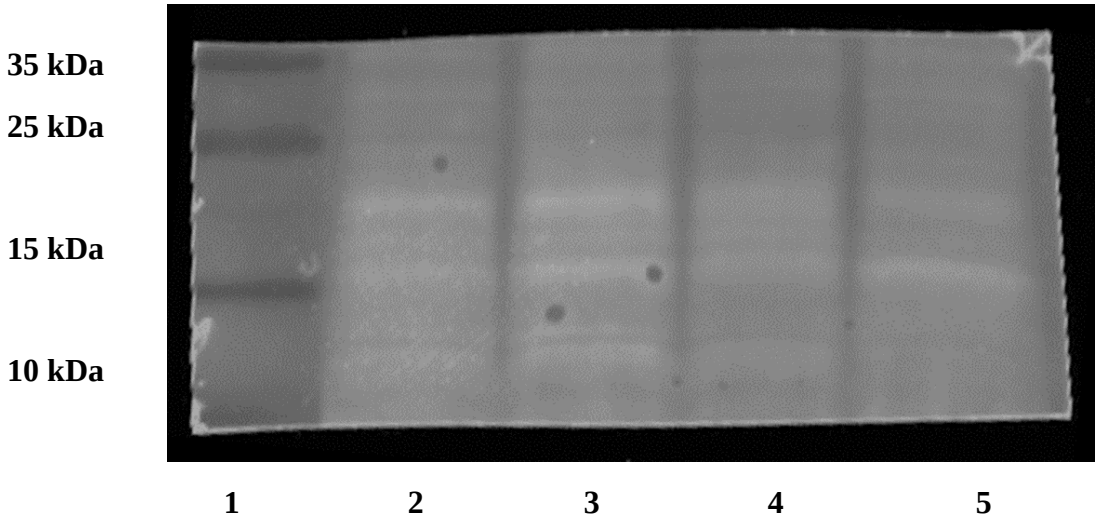


**A:** CC3 Western blot membrane section. Lanes: (1) protein ladder; (2) 0 hour, 0 µM [5-FU]; (3) 8 hour, 10 µM [5-FU]; (4) 16 hour, 10 µM [5-FU]; (5) 24 hour 10 µM [5-FU]. 800 nm excitation. Faint bands at 17 and 19 kDa corresponding to the fragments of CC3 appear slightly more intense than background noise.

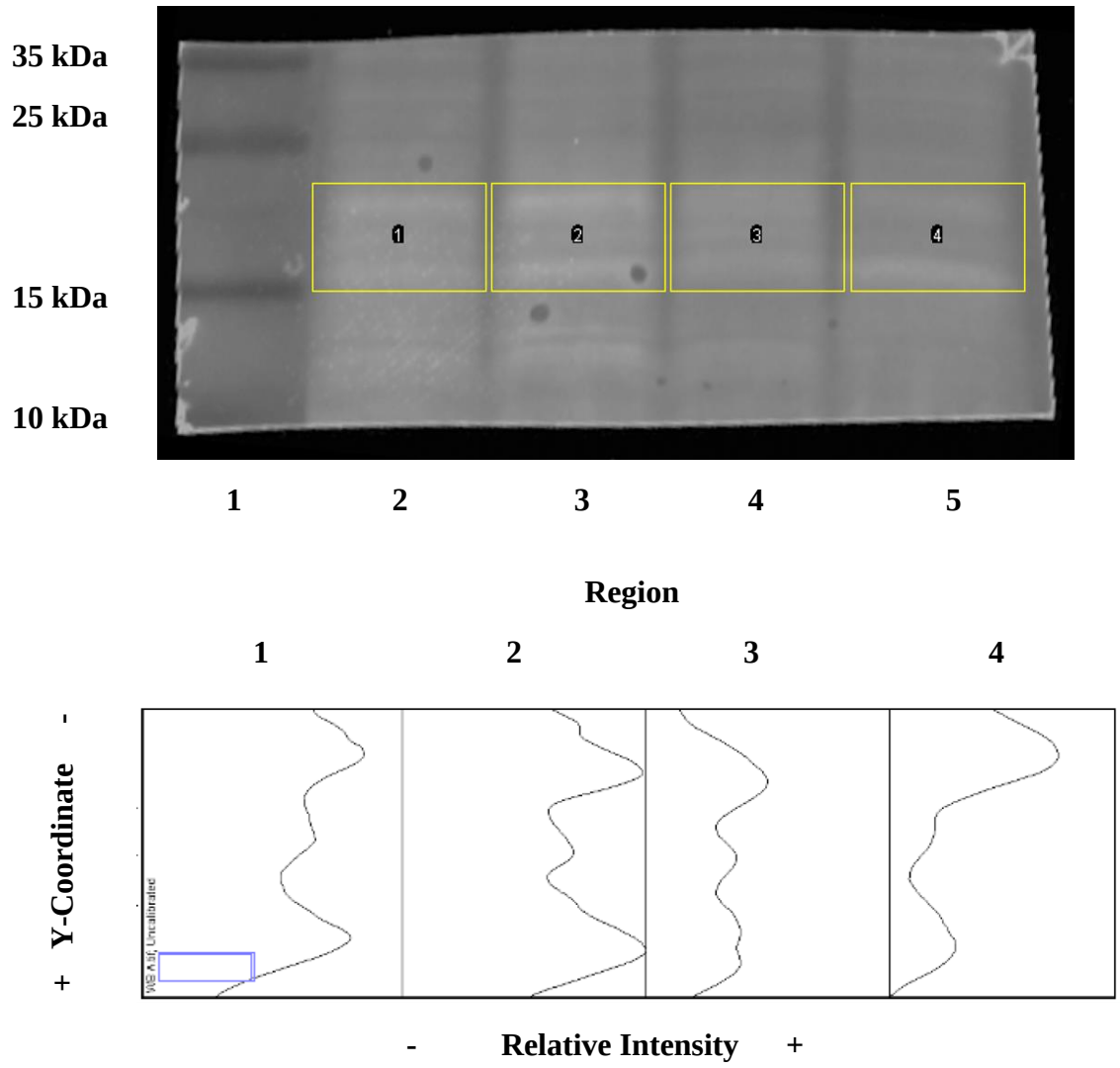


**B: Figure 1:A** WB membrane section showing the band quantification process. The identical regions are shown drawn around each full lane from approximately 15-22 kDa. The plot shows changes in relative intensity moving in the Y direction across each region from the bottom of the region to the top. Intensity peaks separated by regions of lower intensity correspond to CC3 bands at 17 and 19 kDa but appear only slightly more intense than intra-lane background, preventing accurate partitioning of the band area from the background area and thus preventing accurate identification/quantification of CC3 band intensities.

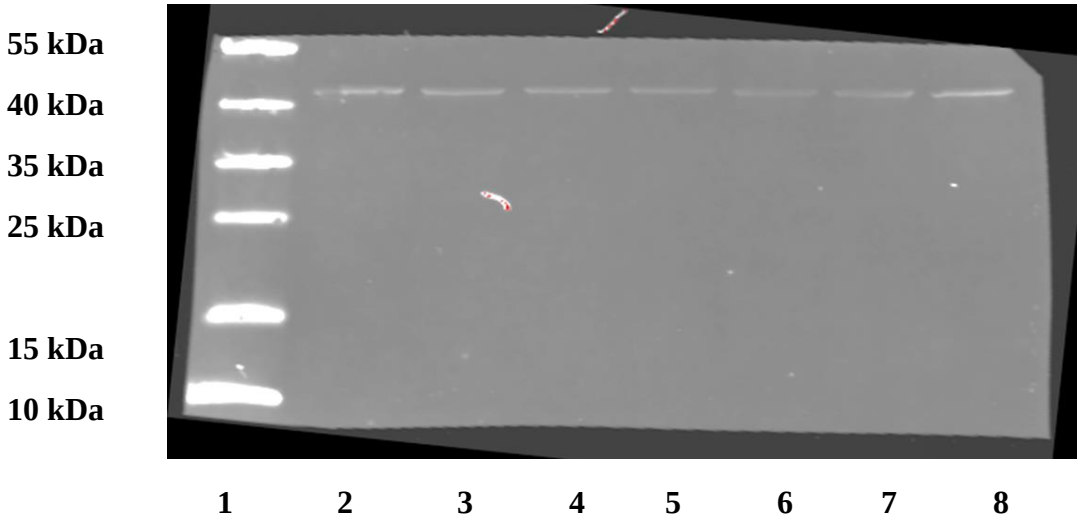


**C:** CC3 Western blot membrane section. Lanes: (1) protein ladder; (2) 0 hour, 0 µM [5-FU]; (3) 12 hour, 0 µM [5-FU]; (4) 12 hour, 10 µM [5-FU]; (5) 12 hour, 20 µM [5-FU]; (6) 24 hour, 0 µM [5-FU]; (7) 24 hour, 10 µM [5-FU]; (8) 24 hour, 20 µM [5-FU]. 700 nm excitation. The bands at approximately 42 kDa correspond to the β-actin loading control and appear clearly, with no bands corresponding to CC3 visible.

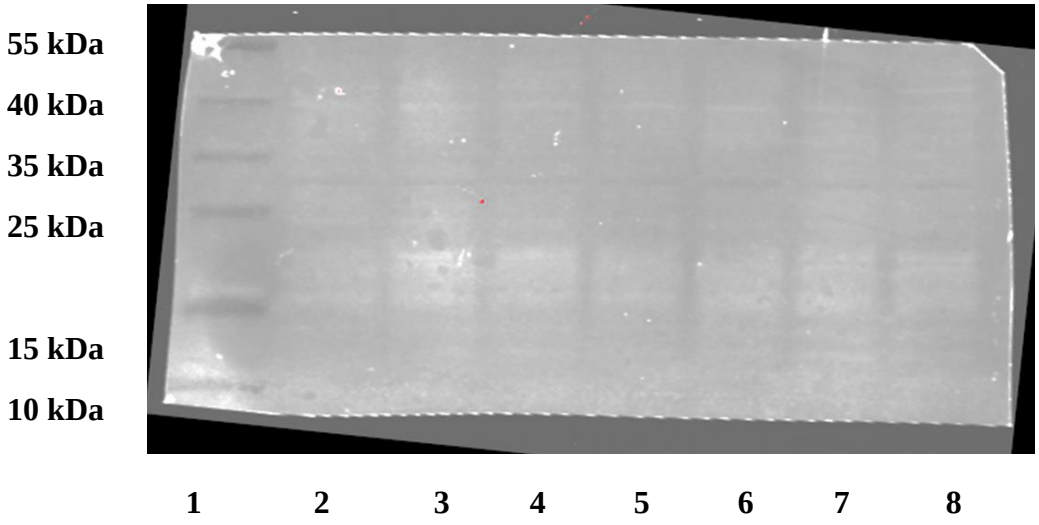


**D: Figure 1:C** Western blot membrane section. 800 nm excitation. The blurry bands around 17 and 19 kDa corresponding to CC3 appear slightly more intense than background noise.

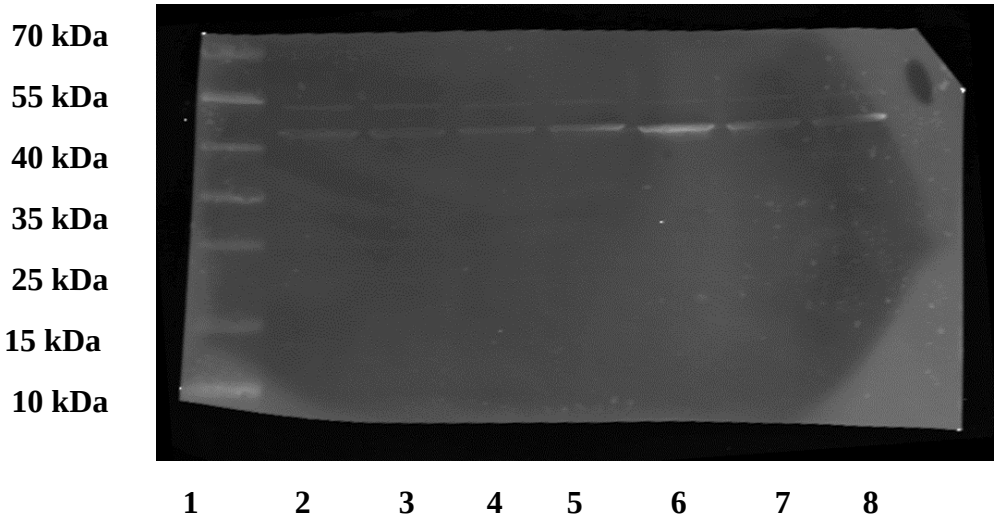


**E:** CC3 Western blot membrane section. Lanes: (1) protein ladder; (2) 0 hour, 0 µM [5-FU]; (3) 12 hour, 0 µM [5-FU]; (4) 12 hour, 10 µM [5-FU]; (5) 12 hour, 20 µM [5-FU]; (6) 24 hour, 0 µM [5-FU]; (7) 24 hour, 10 µM [5-FU]; (8) 24 hour, 20 µM [5-FU]. 700 nm excitation. The bands at 42 kDa corresponding to β-actin loading control appear relatively more intense than background noise, with no bands corresponding to CC3 visible.

**Two-Photon Excitation Fluorescence Microscopy of Redox Ratio**

**Figure 2:** MPM imaging of CRC cells with NADH and FAD autofluorescence and cell cytoplasm segmentation.

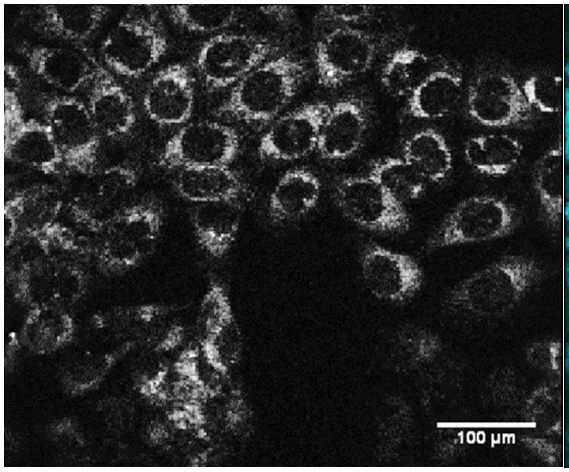


**Figure 2:A:** NADH autofluorescence intensity image.

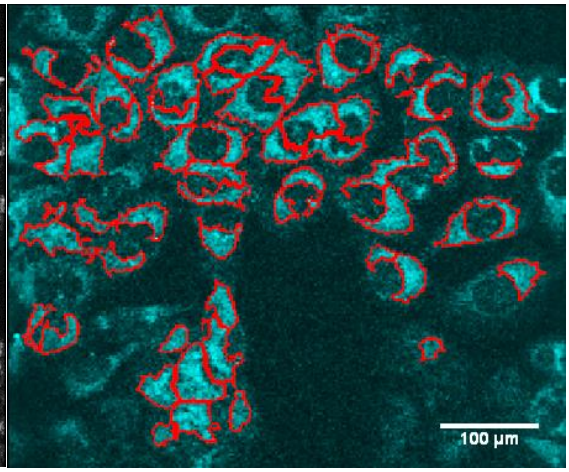


**Figure 2:B:** NADH cell cytoplasm segmentation mask overlaid onto NADH image.

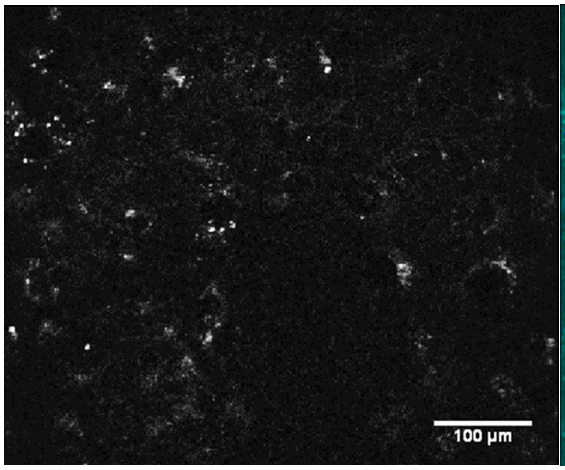


**Figure 2:B:** FAD autofluorescence intensity image.

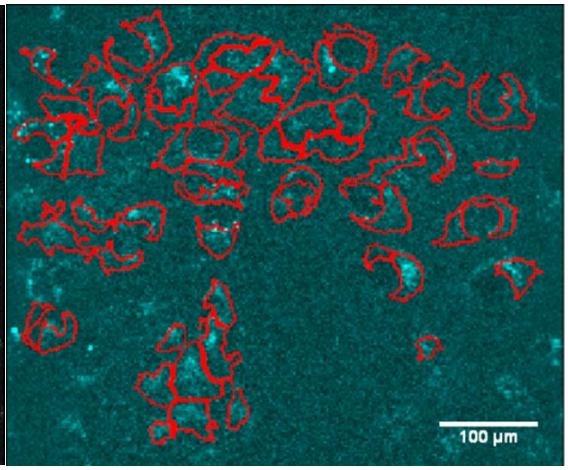


**Figure 2:C:** NADH cell cytoplasm segmentation mask overlaid onto FAD image.

**Figure 3:** CRC cells experience slight changes in redox ratio distribution over the course of 5-FU treatment.

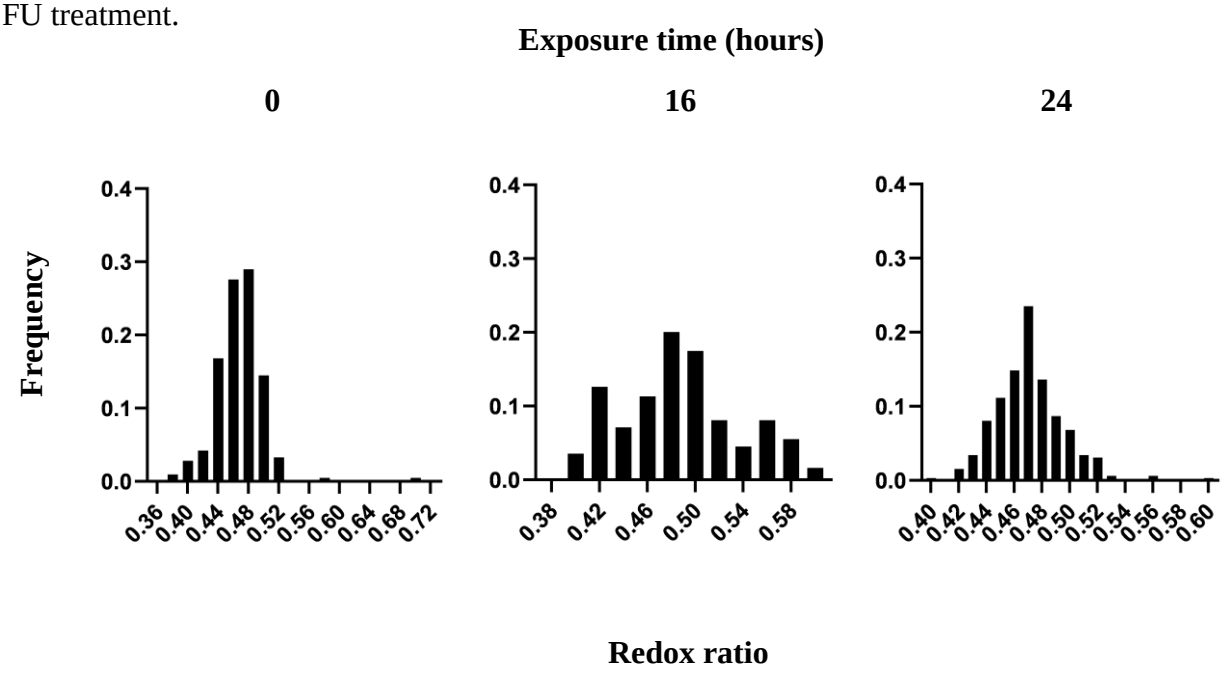


**Figure 3:** Histograms of redox ratio versus fraction of cells for 0-hour (214 cells), 16-hour (309 cells), and 24-hour (324 cells) 10 μM 5-FU treatments. The frequency distribution is graphed as relative frequency (fraction of cells) versus redox ratio. Redox ratio bin number was determined using $Bin\ Number = Log_2(Number\ of\ Redox\ Ratio\ Values\ for\ Given\ Treatment)$. Redox ratio means and standard deviations are as follows: 0-hour treatment: μ=0.467, σ=0.0321; 16-hour treatment: μ=0.488, σ=0.0319; 24-hour treatment: μ=0.471, σ=0.0173.

**Figure 4:** Redox ratio increase to a maximum and then decreases over the course of 5-FU treatment.

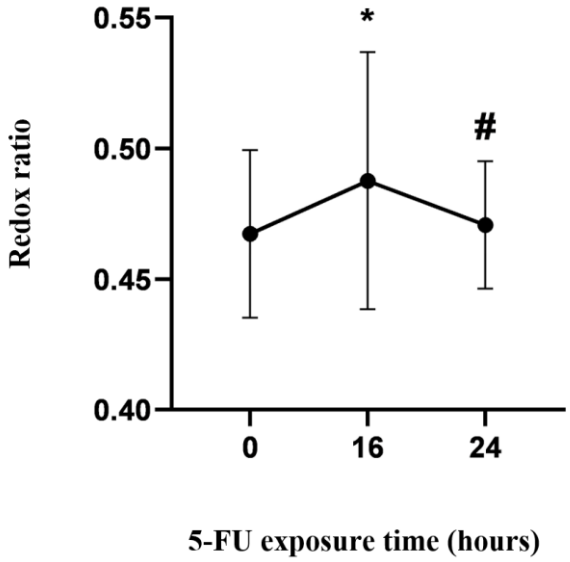


**Figure 4:** Mean and standard deviation of redox ratio values plotted versus 10 µM 5-FU exposure time. A nonparametric ANOVA (Kruskal-Wallis and *post hoc* Dunn's Multiple Comparisons Tests) shows *p-value<0.0001 compared to the 0-hour treatment and #p-value<0.0001 compared to the 16-hour treatment. This test was used because the data is not normally distributed and means of all groups are compared to each other with a Tukey multiplicity-adjusted alpha=0.05.

**Discussion**

Despite extensive optimization and iteration of the CC3 Western blot, the sensitivity of this blot protocol proved too low to accurately quantify CC3 expression through 5-FU exposure time. Intense protein ladder and β-actin control bands suggest SDS-PAGE and transfer were effective. Possible errors preventing intense CC3 bands include high resistance of the HCT116 CRC cell line to 5-FU treatment; however, at 5-FU concentrations of 10 and 20 µM apoptosis should occur. (7,

22) The cell population may have simply been to small to produce adequate amounts of CC3 for detection via Western blot, or, similarly, the CC3 protein fraction may have been a very small fraction of the total protein quantified via BCA assay, affecting Western blot sample preparation. Also, the timepoints selected may not have corresponded well with the apoptosis window in culture and expressed CC3 broke down before lysate collection. (2, 3, 23) Lastly, it is possible the primary and secondary CC3 antibodies used here were simply not specific enough for the amounts of CC3 present. Apoptosis in culture is readily visible with a brightfield microscope; lack of visible apoptotic debris in culture in these experiments suggests the cells were highly resistant to treatment, or the exposure times did not match the apoptosis window well. (2)

Redox ratio values exhibited a significant increase with 5-FU exposure time, followed by a significant decrease back to values not significantly different from the control group. This trend may be explained by MPM images capturing basal CRC redox ratio values at 0 hours of 5-FU exposure; then, after some period of 5-FU exposure, MPM images capture cells undergoing apoptosis and experiencing higher levels of oxidative stress resulting from an increase in reactive oxygen species associated with the apoptosis cascade. (2) After 24 hours of 5-FU exposure, cells with low resistance to 5-FU have undergone apoptosis, leaving high resistance cells with essentially basal CRC oxidative stress and redox ratio. Higher levels of reactive oxygen species would result in an oxidized mitochondrial state, oxidized flavoproteins such as FAD, and an increase in redox ratio. (17)

However, some discrepancies should be noted in the redox ratio imaging methods and results. First, several limitations of redox ratio as an indicator of metabolic activity are ignored in these experiments. Namely, other cellular chromophores with similar excitation and emission spectra to NADH and FAD, such as keratin, lipofuscin, and retinol, may have contributed signal

to NADH and FAD measurements. (21) Secondly, the redox ratio results presented here may be interpreted differently considering a unique cancer metabolic profile—the Warburg Effect. The Warburg Effect describes a reprogramming of cellular metabolism that allows cells to preferentially metabolize glucose, resorting to glycolysis rather than oxidative phosphorylation. This has been explained as a mechanism for rapid ATP generation to support uncontrolled cancer cell proliferation. (14, 24) If the HCT116 CRC cells produce energy mainly by the glycolytic pathway and NADH is considered as the primary metabolic cofactor involved in glycolysis and FAD is considered as essentially isolated to oxidative phosphorylation, then increases in the redox ratio here would indicate an increase in metabolic activity with 5-FU treatment—the opposite of the expected effect. Some research suggests CRC cells employ this glycolytic ATP production. (25, 26) However, even the binary interpretation of redox ratio as either an indicator of oxidative phosphorylation or glycolysis for energy production condones other potential processes such as glutominolysis and fatty acid biosynthesis that may offer further explanation into the actual effects of 5-FU on CRC redox ratio and apoptosis. (21) It remains that a preponderance of evidence shows decreases in redox ratio with chemotherapy, contrary to the result presented here. Increases in redox ratio were, however, associated with changes to a metastatic phenotype in past studies. (14-20)

**Conclusion and Future Directions**

Because of complex tumor biology and interpatient heterogeneity, a need remains to monitor tumor response to therapy at an individual level through real time, sensitive methods in order to minimize negative side effects, expenses, and lack of health benefits associated with ineffective treatments. Then, health workers can identify and proceed with higher-efficacy treatments more efficiently. TPEFM technology provides many advantages over traditional methods for

quantifying tumor response to therapy and may help realize individual cancer care with optical, metabolic imaging of redox ratio. In CRC cells, however, a benchmark of 5-FU induced apoptosis rates should be constructed to corroborate trends in redox ratio. Future experiments should investigate using other apoptosis assays, such as an Annexin V apoptosis assay, or even a combination of assays. (2, 3) Then, a reputable standard of apoptosis in this context of cell line and chemotherapy can be used to evaluate MPM methods. Secondly, redox ratio should be investigated with other assays that shed light on the metabolic profile of the cells so that more concrete results can be reached in terms of the significance of changes in this redox ratio and how those changes might relate to 5-FU induced apoptosis. Combinations of multiple markers to monitor tumor response to treatment, including redox ratio and additional molecular/morphological responses, should be investigated as well. (2, 3) A move toward more physiologically relevant modelling with a 3-D tumor spheroid to better predict results of future in vivo experiments may also prove beneficial. (27) Lastly, the objectives presented here may be extended to other cancer types, quantification of response to novel drugs, and monitoring of dysplastic and metastatic progression.

**Acknowledgements**

I would like to acknowledge Muldoon Lab, the Arkansas Biosciences Institute, The University of Arkansas Honors College, and the National Science Foundation. This research has been supported by an Honors College grant.

**References**

1. Cancer Statistics - National Cancer Institute: National Institute of Health; 2015 [updated 04/02/2015 - 08:00]. Available from: https://www.cancer.gov/about-cancer/understanding/statistics.

2. Weber WA. Assessing tumor response to therapy. J Nucl Med. 2009;50 Suppl 1:1s-10s. Epub 2009/04/22. doi: 10.2967/jnumed.108.057174

10.2967/jnumed.108.057174. Epub 2009 Apr 20. PubMed PMID: 19380403.

3. Zhao B, Schwartz LH, Larson SM. Imaging surrogates of tumor response to therapy: anatomic and functional biomarkers. J Nucl Med. 2009;50(2):239-49. Epub 2009/01/24. doi: 10.2967/jnumed.108.056655

10.2967/jnumed.108.056655. Epub 2009 Jan 21. PubMed PMID: 19164218.

4. Wu S, Huang Y, Tang Q, Li Z, Horng H, Li J, Wu Z, Chen Y, Li H. Quantitative evaluation of redox ratio and collagen characteristics during breast cancer chemotherapy using two-photon intrinsic imaging. Biomed Opt Express. 2018;9(3):1375-88. Epub 2018/03/16. doi: 10.1364/boe.9.001375

10.1364/BOE.9.001375. eCollection 2018 Mar 1. PubMed PMID: 29541528; PMCID: PMC5846538.

5. Key Statistics for Colorectal Cancer: American Cancer Society; 2020. Available from: https://www.cancer.org/cancer/colon-rectal-cancer/about/key-statistics.html.

6. Liu H, Liu X, Zhang C, Zhu H, Xu Q, Bu Y, Lei Y. Redox Imbalance in the Development of Colorectal Cancer. J Cancer2017. p. 1586-97.

7. Alhallak K, Rebello LG, Muldoon TJ, Quinn KP, Rajaram N. Optical redox ratio identifies metastatic potential-dependent changes in breast cancer cell metabolism. Biomed Opt Express. 2016;7(11):4364-74. Epub 2016/11/30. doi: 10.1364/boe.7.004364

10.1364/BOE.7.004364. eCollection 2016 Nov 1. PubMed PMID: 27895979; PMCID: PMC5119579.

8. Pardini B, Kumar R, Naccarati A, Novotny J, Prasad RB, Forsti A, Hemminki K, Vodicka P, Lorenzo Bermejo J. 5-Fluorouracil-based chemotherapy for colorectal cancer and MTHFR/MTRR genotypes. Br J Clin Pharmacol. 2011;72(1):162-3. doi: 10.1111/j.1365-2125.2010.03892.x

10.1111/j.1365-2125.2010.03892.x. PubMed PMID: 21204909; PMCID: 3141199.

9. Miura K, Kinouchi M, Ishida K, Fujibuchi W, Naitoh T, Ogawa H, Ando T, Yazaki N, Watanabe K, Haneda S, Shibata C, Sasaki I. 5-FU Metabolism in Cancer and Orally-Administrable 5-FU Drugs. Cancers (Basel)2010. p. 1717-30.

10. Kaina B. DNA damage-triggered apoptosis: critical role of DNA repair, double-strand breaks, cell proliferation and signaling. Biochem Pharmacol. 2003;66(8):1547-54. Epub 2003/10/14. doi: 10.1016/s0006-2952(03)00510-0

10.1016/s0006-2952(03)00510-0. PubMed PMID: 14555233.

11. Roos WP, Kaina B. DNA damage-induced cell death by apoptosis. Trends Mol Med. 2006;12(9):440-50. Epub 2006/08/11. doi: 10.1016/j.molmed.2006.07.007

10.1016/j.molmed.2006.07.007. Epub 2006 Aug 8. PubMed PMID: 16899408.

12. Watson AJM. Apoptosis and colorectal cancer. Gut2004. p. 1701-9.

13. Multiphoton Fluorescence Microscopy | Olympus Life Science 2020. Available from: https://www.olympus-lifescience.com/en/microscope-resource/primer/techniques/fluorescence/multiphoton/multiphotonintro/.

14. Alhallak K, Rebello LG, Muldoon TJ, Quinn KP, Rajaram N. Optical redox ratio identifies metastatic potential-dependent changes in breast cancer cell metabolism. Biomed Opt Express2016. p. 4364-74.

15. Chance B, Schoener B, Oshino R, Itshak F, Nakase Y. Oxidation-reduction ratio studies of mitochondria in freeze-trapped samples. NADH and flavoprotein fluorescence signals. J Biol Chem. 1979;254(11):4764-71. Epub 1979/06/10. PubMed PMID: 220260.

16. Wu S, Huang Y, Tang Q, Li Z, Horng H, Li J, Wu Z, Chen Y, Li H. Quantitative evaluation of redox ratio and collagen characteristics during breast cancer chemotherapy using two-photon intrinsic imaging. Biomed Opt Express2018. p. 1375-88.

17. Xu HN, Nioka S, Glickson JD, Chance B, Li LZ. Quantitative mitochondrial redox imaging of breast cancer metastatic potential. J Biomed Opt. 2010;15(3). doi: 10.1117/1.3431714

10.1117/1.3431714. PubMed PMID: 20615012.

18. Li LZ, Xu HN, Ranji M, Nioka S, Chance B. MITOCHONDRIAL REDOX IMAGING FOR CANCER DIAGNOSTIC AND THERAPEUTIC STUDIES. J Innov Opt Health Sci. 2009;2(4):325-41. doi: 10.1142/s1793545809000735

10.1142/S1793545809000735. PubMed PMID: 26015810; PMCID: 4442014.

19. Ramanujam MCS, Kristin MR, Annette G-F, Jens E, Kevin WE, John GW, Nirmala. In vivo multiphoton microscopy of NADH and FAD redox states, fluorescence lifetimes, and cellular morphology in precancerous epithelia2007. doi: 10.1073/pnas.0708425104.

20. Skala M, Ramanujam N. Multiphoton Redox Ratio Imaging for Metabolic Monitoring in vivo. Methods Mol Biol. 2010;594:155-62. doi: 10.1007/978-1-60761-411-1_11

10.1007/978-1-60761-411-1_11. PubMed PMID: 20072916; PMCID: 2874879.

21. Varone A, Xylas J, Quinn K. Endogenous Two-Photon Fluorescence Imaging Elucidates Metabolic Changes Related to Enhanced Glycolysis and Glutamine Consumption in Precancerous Epithelial Tissues. Molecular and Cellular Pathobiology. 2014.

22. Dong YF, Yang G, Zhu F, Peng C, Li W, Li H, Kim HG, Bode AM, Dong Z. Antioxidants decrease the apoptotic effect of 5-Fu in colon cancer by regulating Src-dependent caspase-7 phosphorylation. Cell Death & Disease. 2014;5(1). doi: doi:10.1038/cddis.2013.509.

23. Xanthoudakis PT, Hell K, Giroux A, Grimm E, Han Y, Nicholson DW. Catalytic activity of caspase-3 is required for its degradation: stabilization of the active complex by synthetic inhibitors. Cell Death & Differentiation. 2004;11(4):439-47. doi: doi:10.1038/sj.cdd.4401360.

24. Liberti MV, Locasale JW. The Warburg Effect: How Does it Benefit Cancer Cells? Trends Biochem Sci. 2016;41(3):211-8. doi: 10.1016/j.tibs.2015.12.001

10.1016/j.tibs.2015.12.001. PubMed PMID: 26778478; PMCID: 4783224.

25. La Vecchia S, Sebastian C. Metabolic pathways regulating colorectal cancer initiation and progression. Semin Cell Dev Biol. 2020;98:63-70. Epub 2019/05/28. doi: 10.1016/j.semcdb.2019.05.018

10.1016/j.semcdb.2019.05.018. Epub 2019 May 28. PubMed PMID: 31129171.

26. Brown RE, Short SP, Williams CS. Colorectal Cancer and Metabolism. Curr Colorectal Cancer Rep. 2018;14(6):226-41. doi: 10.1007/s11888-018-0420-y

10.1007/s11888-018-0420-y. PubMed PMID: 31406492; PMCID: 6690608.

27. Edmondson R, Broglie JJ, Adcock AF, Yang L. Three-Dimensional Cell Culture Systems and Their Applications in Drug Discovery and Cell-Based Biosensors. Assay Drug Dev Technol2014. p. 207-18.